Biochimica et Biophysica Acta 1797 (2010) 531–542

Contents lists available at ScienceDirect

Biochimica et Biophysica Acta

journal homepage: www.elsevier.com/locate/bbabio

Horseradish peroxidase-catalyzed oxidation of chlorophyll *a* with hydrogen peroxide Characterization of the products and mechanism of the reaction

Paavo H. Hynninen [a,*], Vesa Kaartinen [b,c], Erkki Kolehmainen [d]

[a] Department of Chemistry, Laboratory of Organic Chemistry, P.O. Box 55, A.I. Virtasen Aukio 1, FIN-00014 University of Helsinki, Finland
[b] Developmental Biology, Department of Pathology, Childrens Hospital Los Angeles, 4650 Sunset Blvd., Los Angeles, CA 90027, USA
[c] Department of Biochemistry and Biotechnology, University of Kuopio, P.O. Box 1627, FI-70211 Kuopio, Finland
[d] Department of Chemistry, Laboratory of Organic Chemistry, University of Jyväskylä, P.O. Box 35, FI-40014 Jyväskylä, Finland

ARTICLE INFO

Article history:
Received 2 October 2009
Received in revised form 11 January 2010
Accepted 15 January 2010
Available online 25 January 2010

Keywords:
Enzyme
Peroxidase
Chlorophyll
Allomerization
Oxidation
Free-radical

ABSTRACT

Horseradish peroxidase was verified to catalyze, without any phenol, the hydrogen peroxide oxidation of chlorophyll *a* (Chl *a*), solubilized with Triton X-100. The $13^2(S)$ and $13^2(R)$ diastereomers of 13^2-hydroxyChl *a* were characterized as major oxidation products (ca. 60%) by TLC on sucrose, UV–vis, ^{1}H, and ^{13}C NMR spectra, as well as fast-atom bombardment MS. A minor amount of the 15^2-methyl, 17^3-phytyl ester of Mg-unstable chlorin was identified on the basis of its UV–vis spectrum and reactivity with diazomethane, which converted it to the 13^1,15^2-dimethyl, 17^3-phytyl ester of Mg-purpurin 7. The side products (ca. 10%) were suggested to include the 17^3-phytyl ester of Mg-purpurin 18, which is known to form easily from the Mg-unstable chlorin. The side products also included two red components with UV–vis spectral features resembling those of pure Chl *a* enolate anion. Hence, the two red components were assigned to the enolate anions of Chl *a* and pheophytin *a* or, alternatively, two different complexes of the Chl *a* enolate ion with Triton X-100. All the above products characterized by us are included in our published free-radical allomerization mechanism of Chl *a*, i.e. oxidation by ground-state dioxygen. The HRP clearly accelerated the allomerization process, but it did not produce bilins, that is, open-chain tetrapyrroles, the formation of which would require oxygenolysis of the chlorin macrocycle. In this regard, our results are in discrepancy with the claim by several researchers that 'bilirubin-like compounds' are formed in the HRP-catalyzed oxidation of Chl *a*. Inspection of the likely reactions that occurred on the distal side of the heme in the active centre of HRP provided a reasonable explanation for the observed catalytic effect of the HRP on the allomerization of Chl. In the active centre of HRP, the imidazole nitrogen of His-42 was considered to play a crucial role in the C-13^2 deprotonation of Chl *a*, which resulted in the Chl *a* enolate ion resonance hybrid. The Chl enolate was then oxidized to the Chl 13^2-radical while the HRP Compound I was reduced to Compound II. The same reactive Chl derivatives, i.e. the Chl enolate anion and the Chl 13^2-radical, which are produced twice in the HRP reaction cycle, happen to be the crucial intermediates in the initial stages of the Chl allomerization mechanism.

1. Introduction

Heme (protoheme IX, haem) peroxidases (EC 1.11.1.7: donor: hydrogen peroxide oxidoreductases) represent an extraordinarily large group of heme *b* or modified heme *b* containing oxidative enzymes that use hydrogen peroxide (H_2O_2) or an organic peroxide to oxidize a great variety of both organic and inorganic co-substrates. The quantity of literature dealing with the structure, mechanism, and function of peroxidases, is stunning; several books [1–6], reviews [7–14], and a great number of specific original papers have appeared.

Peroxidases are found widely in biological organisms such as bacteria, fungi, plants, and animals. There are two so-called superfamilies of peroxidases [4]. The animal peroxidases (aka mammalian or human peroxidases), which contain a modified heme *b* as a prosthetic group, represent one superfamily [4,8,15]. The peroxidases, which contain heme *b* as a coenzyme, occur in fungi, bacteria, and plants and form the second superfamily. Using similarity in protein sequence as a criterion, the fungal, bacterial, and plant peroxidases can be divided into three major classes (Table 1) [12]. Table 1 is largely based on the information provided by the review of Veitch [12] and the PROMISE database (© University of Leeds 1998) [14].

Several bacterial catalase-peroxidases (BcatP) are known and have been isolated from both prokaryotic and lower eukaryotic organisms [15]. The *Mycobacterium tuberculosis* catalase-peroxidase (KatG,

Abbreviations: Chl, chlorophyll; Chlide, chlorophyllide; FRA, free-radical allomerization; HO, hydroxy; HRP, horseradish peroxidase; HRPC, HRP isoenzyme C; HRP-I, HRP Compound I; HRP-II, HRP Compound II; LP, light petroleum; NCC, nonfluorescent Chl catabolite; PaO, pheophorbide *a* oxygenase; pFCC, primary fluorescent Chl catabolite; Pheo, pheophytin; Pheide, pheophorbide; Phy, phytyl; Porph, porphyrin; PTI, phase-test intermediate; Pyro, 13^2-demethoxycarbonyl; RCC, red Chl catabolite; RCCR, RCC reductase; RH, reducing substrate; *R*, *S*, absolute configurations of chiral centres

* Corresponding author. Tel.: +358 9 19150358; fax: +358 9 19150466.
E-mail address: paavo.hynninen@helsinki.fi (P.H. Hynninen).

0005-2728/$ – see front matter © 2010 Elsevier B.V. All rights reserved.
doi:10.1016/j.bbabio.2010.01.017

Table 1
Classification of fungal, bacterial, and plant peroxidases with examples of enzymes and their characteristics.

Class	Examples	Characteristics
I	Yeast (*Saccharomyces cerevisiae*) cytochrome *c* peroxidase (CcP); ascorbate peroxidase (AP); bacterial catalase-peroxidases (BcatP); e.g. *Mycobacterium tuberculosis* BcatP (KatG, S315T).	These are intracellular peroxidases, lacking disulphide bridges, carbohydrate, calcium, and a signal sequence for endoplasmic reticulum; CcP is a soluble protein occurring in the mitochondrial electron transport chain and probably protecting against toxic peroxides; AP is the main enzyme responsible for removal of H_2O_2 from chloroplasts and cytosol of higher plants; BcatPs show both catalase and peroxidase activities and are thought to provide protection to cells under oxidative stress. For CcP, the cation radical of Compound I is located at the Trp 191 residue of the protein; for AP and BcatB, the cation radical of Compound I is located at the porphyrin macrocycle.
II	*Coprinus cinereus* peroxidase; Lignin peroxidase (LiP) or ligninase and manganese peroxidases (MnP) of *Phanerochaete chrysosporium* and *Trametes versicolor*.	These are secretory (extracellular) fungal peroxidases, involved in the degradation of lignin; Class II peroxidases are monomeric glycoproteins, containing an *N*-terminal signal peptide, carbohydrate, two conserved calcium sites, four conserved disulphide bridges (located differently from class III peroxidases), and a C-terminal domain of 40–60 amino acid residues, absent from Class I and Class III peroxidases; The cation radical of Compound I is located at the porphyrin macrocycle; In MnP, Mn^{2+} serves as the reducing substrate.
III	Horseradish (*Armoracia rusticana*) peroxidase (HRP); thale cress (*Arabidopsis thaliana*) peroxidase (AtP); peanut (*Arachis hypogaea*) peroxidase (PNP); soybean (*Glycine max*) peroxidase (SBP); barley (*Hordeum vulgare*) peroxidase (BP).	These are secretory or classical plant peroxidases, which have multiple tissue-specific functions: e.g., removal of H_2O_2 from chloroplasts and cytosol, oxidation of toxic compounds, biosynthesis of the cell wall, defence responses towards wounding, catabolism of the indole acetic acid (IAA) plant hormone, biosynthesis of the ethylene plant hormone; Class III peroxidases are monomeric glycoproteins, containing four conserved disulphide bridges, two conserved calcium binding sites, an *N*-terminal signal peptide, and some members have a C-terminal propeptide that may target to vacuoles; The cation radical of Compound I is located at the porphyrin macrocycle.

S315T) was selected as an example in Table 1 owing to its medicinal interest [16] and exceptional catalytic properties. Besides catalase and peroxidase activities, KatG is reported to possess Mn^{2+}-dependent peroxidase, cytochrome P450-like oxygenase, and peroxynitritase activities [16].

The peroxidases catalyze biological oxidation reactions, involving similar high oxidation state ($Fe^{IV}=O$, oxoferryl) intermediates, whose reactivities are modulated by the protein environment. Many synthetic applications of peroxidases have already been published in the field of enzyme-catalyzed organic synthesis [17–21]. Horseradish peroxidase (HRP) is a Class III peroxidase (Table 1), found and purified from the root of horseradish by Keilin and Hartree in 1951 [22]. The crystal structure of HRP isoenzyme C (HRPC) has been solved at 2.15 Å resolution by Gajhede et al. [23]. The results from their study show that HRPC is unique in having three Phe residues on the distal side of the heme, which guard the substrate access channel to the exposed heme edge. The authors predict that these aromatic Phe residues are important for the ability of HRPC to bind aromatic substrates. The peroxidase cycle of the reaction mechanism of HRP consists of the following reactions [23–28]:

$$\underset{\text{Resting state}}{\mathrm{HRP}\left(\mathrm{Fe}^{3+}\right)}\mathrm{Porph} + \mathrm{H_2O_2} \xrightarrow{k_1} \underset{\text{Compound I}}{\mathrm{HRP}\left(\mathrm{Fe}^{4+}=\mathrm{O}\right)}\mathrm{Porph}+\bullet + \mathrm{H_2O} \quad (1)$$

$$\underset{\text{Compound II}}{\mathrm{HRP}\left(\mathrm{Fe}^{4+}=\mathrm{O}\right)}\mathrm{Porph}+\bullet + \mathrm{RH} \xrightarrow{k_2} \mathrm{HRP}\left(\mathrm{Fe}^{4+}=\mathrm{O}\right)\mathrm{Porph} + \mathrm{R}\bullet \quad (2)$$

$$\mathrm{HRP}\left(\mathrm{Fe}^{4+}=\mathrm{O}\right)\mathrm{Porph} + \mathrm{RH} \xrightarrow{k_3} \underset{\text{Resting state}}{\mathrm{HRP}\left(\mathrm{Fe}^{3+}=\mathrm{O}\right)}\mathrm{Porph} + \mathrm{R}\bullet \quad (3)$$

The overall reaction is thus:

$$\mathrm{H_2O_2} + 2\,\mathrm{RH} \xrightarrow{\mathrm{HRP}} 2\mathrm{H_2O} + 2\mathrm{R}\bullet. \quad (4)$$

In these reactions RH represents the co-substrate, i.e. reducing substrate and R• is a free-radical product.

The structure of the HRP Compound I (HRP-I) is best described as a low-spin ($S=1$) oxoferryl porphyrin π-cation radical [29–32]. Thus HRP-I has two oxidizing equivalents above the resting enzyme: one is stored as a low-spin ferryl iron (Fe^{IV}) and the other as a π-cation radical of the porphyrin macrocycle. HRP-I is unstable and spontaneously transforms into HRP Compound II (HRP-II) by abstracting a hydrogen atom (H^+, e^-) from the RH reducing substrate, producing the R• radical. Also HRP-II possesses the oxoferryl group, but it has lost the radical character of its porphyrin macrocycle [33,34]. HRP-II is capable of abstracting both a proton and an electron from RH, yielding the original, resting HRP and the R• radical as oxidized co-substrate.

The peroxidase enzymes, including numerous isoenzymes, occur in the chloroplasts, vacuoles, and associated with the cell walls of plant cells and have been thought to be involved in the biodegradation pathway(s) of chlorophylls during senescence. In the earlier literature on catabolism in plants, many researchers have proposed that oxidizing enzymes, such as 'Chl peroxidase' [35–40], 'Chl oxidase' [40–46], or 'lipoxygenase' [47], are responsible for the type I peripheral oxidative degradations and/or the type II degradations, involving the oxygenolytic cleavage of the chlorin macrocycle and subsequent degradation to monopyrroles, and finally to smaller carbon and nitrogen fragments; see the reviews by Hendry et al. [48] and Brown et al. [49]. The fading or disappearance of green colour ('bleaching' or 'photobleaching') has frequently been interpreted as involving total Chl degradation of type II. More recently, several researchers have proposed that peroxidases can catalyze the type II degradation of chlorophylls (Fig. 1, **1** and **5**) in pathways where $13^2(S/R)$-HO-Chl *a* (**3**/**4**) [50,53,54], PyroPheide *a* (**13**) [51,52], a 'bilirubin-like compound' [50,53,54], and monopyrroles [51,52] are possible intermediates. These proposals are in disharmony with the so-called pheophorbide *a* oxygenase (PaO) degradation pathway of chlorophylls (Scheme 1), worked out and well documented during the past two decades by several Middle European working groups; see the reviews by Gossauer [55], Gossauer and Engel [56], Matile et al. [57,58], Kräutler and Matile [59], Hörtensteiner and Kräutler [60], Takamiya et al. [61], and Hörtensteiner [62].

It is noteworthy that the molecular structures of *Brassica napus* in Scheme 1 do not have a hydroxyl group at the C-13^2 position of the isocyclic ring E. The C-13^2 hydroxyl group is also missing from all the intermediate and NCC structures originating in many other plants

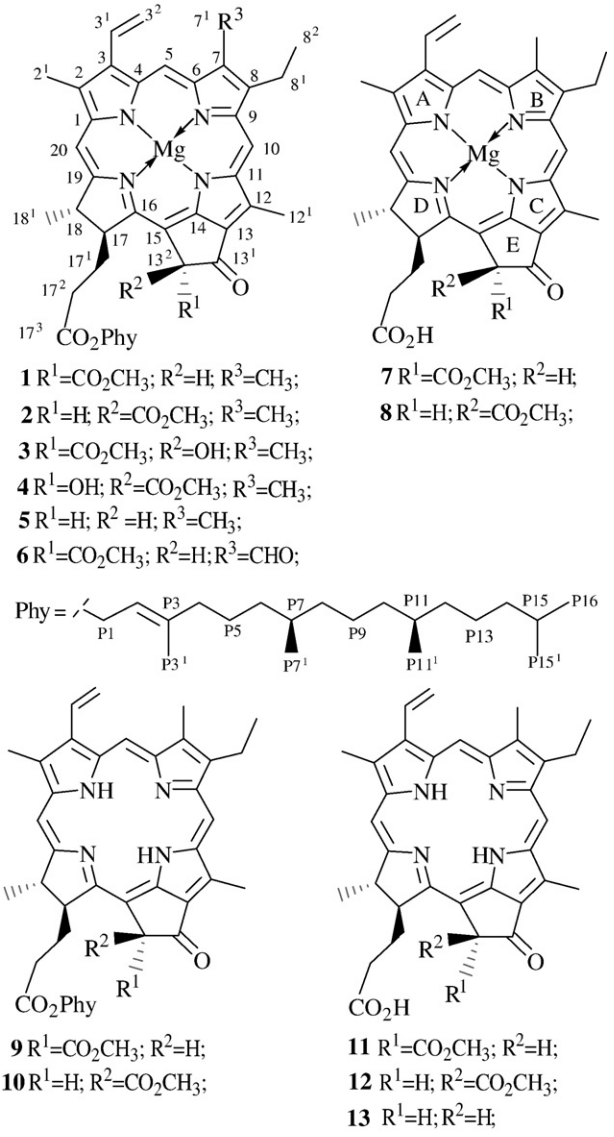

Fig. 1. Structures and semisystematic numbering system [63] of 13^2(*R*)-Chl *a* (**1**), 13^2(*S*)-Chl *a* (**2**), 13^2(*S*)-HO-Chl *a* (**3**), 13^2(*R*)-HO-Chl *a* (**4**), PyroChl *a* (**5**), 13^2(*R*)-Chl *b* (**6**), 13^2(*R*)-Chlide *a* (**7**), 13^2(*S*)-Chlide *a* (**8**), 13^2(*R*)-Pheo *a* (**9**),13^2(*S*)-Pheo *a* (**10**), 13^2(*R*)-Pheide *a* (**11**), 13^2(*S*)-Pheide *a* (**12**) and PyroPheide *a* (**13**).

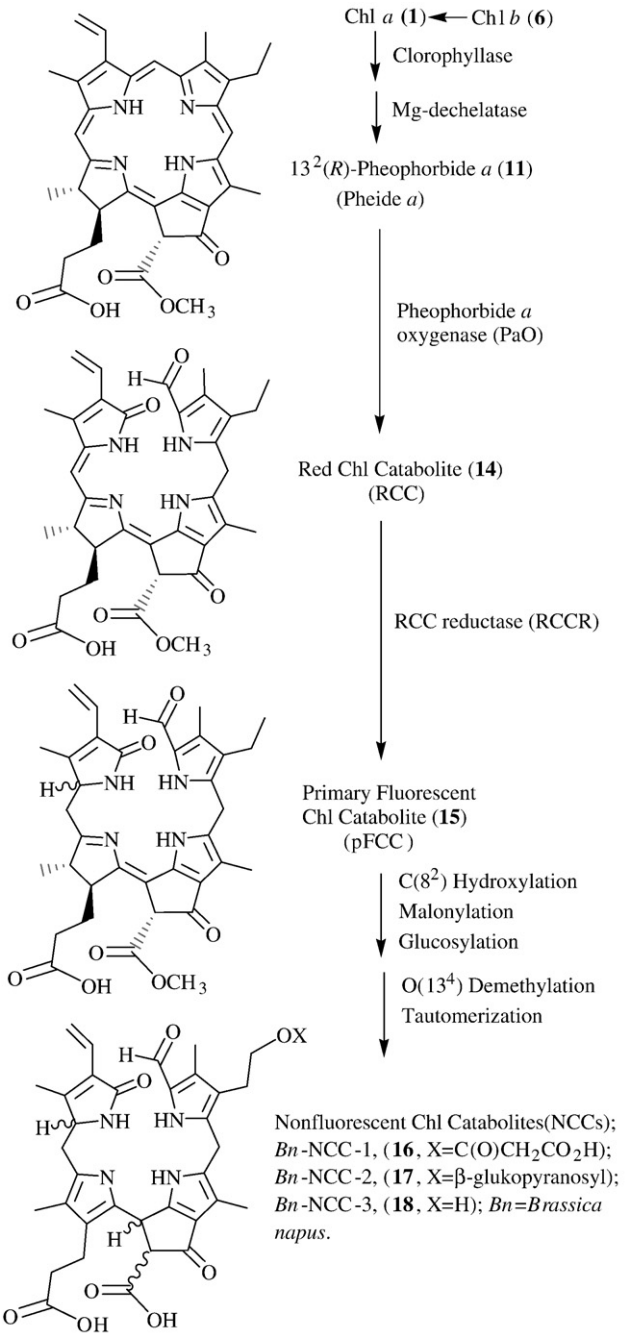

Scheme 1. Proposed degradation pathway for Chl *a* and Chl *b* with Pheide *a*, RCC, and pFCC as intermediates. The reaction sequence produces NCCs as final products, stored in the vacuoles of plant cells. Adapted from Hörtensteiner and Kräutler [60].

[58,62]. In addition, the 13^2-methoxycarbonyl or 13^2-carboxyl group is present in all the intermediates and final NCC structures so far characterized [58,62]. Hence, in these respects, the proposed PaO-catalyzed degradation pathways do not conform to the presumed peroxidase-catalyzed degradation pathways, including 13^2(*S*/*R*)-HO-Chl *a* and PyroPheide *a* as possible intermediates in the pathways [50–54]. Nevertheless, it should also be noted that, until now, it has not been possible to purify the PaO and RCCR enzymes to a high degree, because these are located as a multienzyme complex in the thylakoid membranes of chloroplasts (generally, the membrane enzymes are difficult to purify) [62]. Consequently, as the actual substrate specificity of the PaO remains unknown, it is impossible to know whether 13^2(*S*/*R*)-HO-Pheide *a* or PyroPheide *a* could act as a substrate for PaO in plant species, where this enzyme might be species specific.

The studies performed with the intention to elucidate the role of the 'Chl peroxidase', 'Chl oxidase', or 'lipoxygenase' in the breakdown of chlorophylls, leave many questions unanswered. Apparently, one main reason for this situation is a consequence of the fact that in very few cases, the oxidation products have been properly isolated and structurally characterized. We have found only one work that meets the requirements of an acceptable identification of the oxidation products, formed in vivo from endogenous Chls in barley thylakoids as a result of the action of 'Chl peroxidase' or 'Chl oxidase' [46]. In addition, it should be noted that the terms 'bleaching' and 'photobleaching' are diffuse terms, which do not necessarily mean cleavage and destruction of the chlorin macrocycle. Without opening the macrocycle, one only needs to abstract, chemically or photochemically, one electron from the delocalized, aromatic π-electron system of Chl *a* or *b* to produce a Chl π-cation radical, $Chl^{+\cdot}$. This molecular species has a yellow colour in solution and a distinctly different UV–vis absorption spectrum as compared with that of the original Chl [64,65]. A further example is provided by the 13^2-deprotonation of Chl *a* or *b* (i.e. abstraction of one proton, H^+, from the C-13^2 position),

which gives the enolate anion of Chl. In pure state in pyridine solution, this fascinating molecular species has a colour of red-wine, corresponding to an electronic absorption spectrum (vide infra Fig. 7), which differs markedly from that of the original Chl [66–73].

The purpose of our investigation, to be described here, was to throw some light on the problem, concerning the role of peroxidase enzymes in the degradation of Chls. As noted above, the peroxidase hypothesis has been persistent among many scientists, some of whom still seem to believe that the peroxidase-catalyzed reaction pathway provides an alternative route for the biodegradation of Chls, which is different from the PaO and RCCR catalyzed route. In our work plan, we chose reaction conditions otherwise comparable to those employed by Huff [36], Martinoia et al. [37], and by Kato and Simidzu [38,39], but different in that: (1) We used purified, commercially purchased HRP enzyme instead of HRP-containing biological preparations, such as an extract from barley chloroplast thylakoids [37], or an acetone powder extract, prepared from orange flavedo [36], or tobacco leaves [38]; (2) No phenol was added to the reaction mixture to see whether the presence of a phenol is a prerequisite for the HRP-catalyzed oxidation as claimed by Huff [36], Martinoia et al. [37], and Kato and Simidzu [38]. In addition, the phenol was omitted to see whether HRP has Mg-dechelatase activity as proposed by Azuma et al. [53]; (3) The reaction products were isolated and purified using a mild separation technique on a sucrose column [74,75], or sucrose TLC plate [76]; and (4) The structures of the reaction products were determined by means of electronic absorption spectroscopy (UV–vis), NMR spectroscopy, fast-atom bombardment (FAB) mass spectrometry, and analytical TLC on sucrose plates, applying co-elution with standard preparations of various Chl derivatives from our collection. An abstract dealing with the main products from the HRP-catalyzed oxidation of Chl *a*, was presented at the 9th National NMR Symposium, held in Joensuu, Finland: V. Kaartinen, E. Kolehmainen, P.H. Hynninen, Peroxidase-catalyzed oxidation of chlorophyll *a*: ^{1}H NMR spectroscopic characterization of the principal products as 10(*R*)- and 10(*S*)-hydroxychlorophyll *a*, T. Pakkanen (Ed.), 9th National NMR Symposium Abstracts, Report Series No. 3, University of Joensuu, Joensuu, 1985, pp. 10–12.

2. Materials and methods

2.1. Reagents, solvents, and preparation of Chl a

Horseradish peroxidase (HRP, donor:H_2O_2 oxidoreductase, EC 1.11.1.7) was purchased from Boehringer–Mannheim (HRP, grade II, contained ca. 90% of the isoenzyme C and 10% of isoenzymes A and B). Guaiacol was from Sigma (Q-5502) and H_2O_2 from Merck (Perhydrol®, >30%). NaCl, $K_2HPO_4 3H_2O$, and KH_2PO_4 were of Merck's analytical grade purity. The solvents, such as acetone, isopropanol (2-PrOH), chloroform (stabilized with 2-methyl-2-butene), cyclohexane, and Et_2O (dried, stabilized with butylated hydroxytoluene, BHT) were of Merck's analytical grade purity and were used as provided, except that chloroform was dried with silica gel. Merck's analytical grade light petroleum, LP (60–80 °C) was found to contain at high temperature boiling impurities, which were removed by distilling the LP through a Vigreux column. Acetone-d_6 was purchased from Fluka (0.7 mL ampoules, *d*% 99.95) or from Merck (0.5 mL ampoules, *d*% >99.8) and tetramethylsilane (TMS) from Aldrich. Silica gel 60 (particle size 0.063–0.200 mm, 70–230 Mesh ASTM) was purchased from Merck and sucrose from Finnsugar Ltd, Suomen Sokeri Oy, FI-02460 Kantvik, Finland. This sucrose had the following properties: mean particle size 0.035 mm, sucrose 98.4%, water 0.10%, tricalcium phosphate 1.5%, and sulphur dioxide max. 10 mg/kg.

Dehydrated, solid Chl *a* (Fig. 1, **1**) was prepared by the method described earlier [74], adapted for large-scale preparation. The purity of the Chl preparation was ascertained by electronic absorption spectra [77], ^{1}H NMR spectra [77], and TLC on sucrose [76]. The spectroscopic properties of the preparation were identical with those described previously [77]. The ^{1}H NMR spectra showed water as the only impurity (present in a ratio smaller than 1:1). The sucrose TLC with fluorescence detection under UV light ($\lambda = 366$ nm) revealed trace amounts of Chl *a*′ [13^2(*S*)-Chl *a*] and Pheo *a* in the Chl *a* preparation. Standard Chl *a* derivatives were prepared as described earlier [76].

2.2. Solubilization of Chl a

Chl *a* was dissolved in a small amount of diethyl ether and the solution was transferred over 0.1 M potassium phosphate buffer, pH 5.9, containing 0.25% Triton X-100. The diethyl ether was carefully evaporated at reduced pressure in a Büchi rotary evaporator. The existence of Chl *a* in monomeric form was ascertained by comparing the electronic absorption spectrum of Chl *a* in the detergent solution with the spectrum of Chl *a* in Et_2O.

2.3. Activity assay of HRP

Potassium phosphate buffer, 0.1 M, pH 7.0 (3.0 mL) was pipetted into a cuvette (light path 10 mm) and guaiacol solution, 18 mM (0.05 mL) and HRP preparation, 0.05 mg mL^{-1} (0.02 mL) were added. The reaction was initiated by adding H_2O_2 solution, 8.0 mM (0.04 mL). The change of absorbance at 436 nm per min was measured and the specific activity of HRP calculated according to the instructions by Boehringer–Mannheim. The spectrophotometric measurement gave as specific activity 87 U mg^{-1}.

2.4. Optimal conditions for the HRP-catalyzed oxidation of Chl a with H_2O_2

The optimal [H_2O_2] was determined by fixing the [Chl *a*] to 38 μM and the [HRP] to 1 μM (22 U) while varying the [H_2O_2] between 249 μM and 830 μM. The samples were incubated for 24 h at room temperature in the dark. The optimal [H_2O_2] was found to be 491 μM. Then the optimal [HRP] was determined by fixing the [Chl *a*] to 38 μM and the [H_2O_2] to 491 μM while varying the [HRP] between 0.2 μM (4.4 U) and 2.1 μM (44 U). The optimal [HRP] was found to be 1.0 μM when [Chl *a*] and [H_2O_2] were 38 μM and 491 μM, respectively. These conditions were used in the enzymatic oxidation experiments of Chl *a*.

2.5. Involvement of HRP and H_2O_2 in the oxidation of Chl a

The involvement of the HRP enzyme in the reaction was verified by a test series with the following samples: (a) 38 μM Chl *a* in 0.1 M phosphate buffer, pH 5.9, containing 0.25% of Triton X-100; (b) 38 μM Chl *a* and 491 μM H_2O_2 in the phosphate buffer; (c) 38 μM Chl *a* and 1.0 μM HRP in the phosphate buffer; and (d) 38 μM Chl *a*, 1.0 μM HRP, and 491 μM H_2O_2 in the phosphate buffer. The change of the absorption spectrum of each sample was followed during 24 h on a Cary 219 spectrophotometer. The reactions were carried out at room temperature in the dark. After 24 h, the pigments were extracted into diethyl ether, the detergent was removed and the TLC analysis performed.

2.6. Removal of detergent

Triton X-100 had to be removed, because the chromatographic separation of the oxidation products was impossible in the presence of the detergent. The oxidation products were extracted into diethyl ether. The extraction was promoted by saturating the buffer with sodium chloride. The diethyl ether extract was evaporated to dryness and ice-cold acetone was added to the residue to disintegrate the complexes. The mixture was then applied to a silica gel column (i.d. 2.5 cm, height of the silica gel layer 45 cm). The column was eluted with cold acetone. The detergent-free reaction products were preserved in frozen cyclohexane at −20 °C in the dark for subsequent use.

2.7. Separation of the reaction products by TLC on sucrose and CC on sucrose

The TLC separations were performed in dimmed light on self-made sucrose plates [76]. The samples in acetone were spotted with a capillary onto a sucrose TLC plate. The eluent was 1% 2-PrOH in light petroleum (LP, bp 60–80 °C). After the solvent front had ascended ca. 16 cm, the plates were allowed to dry. The densitogram was measured by a Shimadzu CS-930 densitometer (wavelength 660 nm).

The column chromatographic (CC) separations on sucrose were carried out using a glass column with an inside diameter of 2.5 cm and a height of 50 cm. To prevent evaporation of organic solvents and to make working with flammable organic solvents safe, the upper end of the column, having a ground-glass joint adapter, was connected with Teflon tubing to the solvent bottle. The lower end of the column was similarly connected with Teflon tubing to a receiver bottle. The column was packed with powdered sugar (for properties, see part 2.1). The sugar was passed through a 180 μm sieve and mixed with the eluent (1% 2-PrOH in LP) to form a suitable suspension, which was poured into the column. The sugar was allowed to settle while occasionally rotating the column in an upright position clockwise and counter-clockwise about its long axis. The sugar layer was made compact by allowing eluent to flow through it until no settling movement was observed. Addition of sugar suspension was continued until a final height of 45 cm was reached for the layer. The packed sugar column was connected to a system made up of a flow-through cuvette with a light-path thickness of 1.0 mm, a spectrophotometer, a recorder, and a fraction collector. The mixture of the Chl reaction products in a minimal amount of Et_2O was applied onto the top of the sucrose layer and the column was eluted with 1.0% 2-PrOH in light petroleum. To get the most polar reaction products out of the column, the polarity of the eluent was increased first to 3% 2-PrOH in LP and then to 5% 2-PrOH in LP. To prevent any effects of light on the photosensitive pigments, the sugar column was wrapped with aluminium foil during the separations.

2.8. Identification of the reaction products

2.8.1. UV–vis spectroscopy and TLC

Judging from the elution profile and the absorption spectra, all those fractions, which contained as pure components as possible, were combined. The electronic absorption spectrum of each combined fraction was recorded in Et_2O on a Cary Model 219 spectrophotometer at room temperature. Each combined fraction was also analyzed, after removal of the detergent, by TLC on sucrose with 1% 2-PrOH in LP as eluent [76].

2.8.2. Recording of NMR spectra and mass spectra

The 200 MHz ^{1}H, 50 MHz $^{13}C\{^1H\}$, distortionless enhancement by polarization transfer (DEPT), and $^1H,^{13}C$-heteronuclear NMR spectra of the main oxidation products were recorded on a Varian Gemini FT instrument. The ^{1}H NMR spectra were also recorded with a Bruker 250 MHz instrument. The NMR sample was prepared by dissolving in a 5 mm NMR tube ca. 10 mg of purified Chl derivative in 0.7 mL of acetone-d_6 (ampoules from Fluka, 0.7 mL, *d%* 99.95 or from Merck, 0.5 mL, *d%* 99.8). Tetramethylsilane (TMS) was used as an internal reference. The fast-atom bombardment mass spectra (FAB-MS) were measured with a Finnigan MAT 95 mass spectrometer as described in the literature [78].

2.8.3. Spectrometric data of the main oxidation products

*2.8.3.1. 13^2(S)-Hydroxychlorophyll a (**3**).* ^{1}H NMR (acetone-d_6), δ_H [ppm]: 9.79 (s, 10-CH), 9.46 (s, 5-CH), 8.62 (s, 20-CH), 8.14 (dd, $^3J_{cis}$ = 11.6 Hz, $^3J_{trans}$ = 17.9 Hz, 3^1-CH), 6.22 (dd, $^2J_{gem}$ = 1.8 Hz, $^3J_{trans}$ = 17.9 Hz, 3^2-CH_2, H_{trans}), 6.02 (dd, $^2J_{gem}$ = 1.8 Hz, $^3J_{cis}$ = 11.6 Hz, 3^2-CH_2, H_{cis}), 6.05 (s, 13^2-COH), 5.22 (tq, $^3J_{P2-P1}$ = 7.2 Hz, $^4J_{P2-P3^1}$ = 1.2 Hz, P2-CH), 4.18–4.10 (m, 17-CH), 4.55 (q, $^3J_{18-18^1}$ = 7.2 Hz, 18-CH), 4.53–4.45 (m, P1-CH_2, H_a, H_b), 3.83 (q, $^3J_{8^1-8^2}$ = 7.6 Hz, 8^1-CH_2), 3.64 (s, 12^1-CH_3), 3.58 (s, 13^4-CH_3), 3.36 (s, 2^1-CH_3), 3.31 (s, 7^1-CH_3), 2.90–2.08 (m, 17^1-CH_2, 17^2-CH_2)[a], 1.96–1.82 (m, P4-CH)[b], 1.71 (t, $^3J_{8^2-8^1}$ = 7.6 Hz, 8^2-CH_3), 1.56 (d, $^3J_{18^1-18}$ = 7.2 Hz, 18^1-CH_3), and 1.62 (d, $^4J_{P2-P3^1}$ = 1.2 Hz, P3^1-CH_3); [a]Needs spin simulation for the fragment 17-CH–17^1-CH_2–17^2-CH_2; [b]The assignments of the phytyl P5–P16 proton signals were similar to those reported elsewhere [79]. $^{13}C\{^1H\}$ NMR (acetone-d_6), δ_C [ppm]: 193.41 (13^1), 173.91 (17^3), 170.36 (19), 162.88 (14), 158.75 (16), 156.03 (1), 152.93 (6), 147.32 (9), 149.17 (4), 148.76 (11), 145.40 (8), 143.15 (P3), 140.40 (3), 136.56 (2), 135.20 (7), 135.48 (12), 131.77 (3^1), 129.74 (13), 120.62 (3^2), 119.85 (P2), 109.72 (15), 108.51 (10), 101.34 (5), 94.49 (20), 91.03 (13^2), 61.64 (P1), 52.18 (17), 49.95 (18), 40.45 (P4), ~31.07 (17^1), ~31.07 (17^2), 23.45 (18^1), 20.02 (8^1), 18.07 (8^2), 16.30 (P3^1), 12.78 (12^1), 12.58 (2^1), and 11.17 (7^1); the assignments of the phytyl P5–P16 carbon signals were similar to those reported elsewhere [79]. FAB-MS: *m/z* 908.4 [$M^{+\cdot}$]; $C_{55}H_{72}N_4O_6Mg$ requires 908.5. UV–vis in Et_2O: λ_{max} (relative intensity) at 661.6 (0.847), 614.5 (0.139), 573.5 (0.076), 530.3 (0.043), 429.3 (1.000) and 410.9sh (0.761) nm (Table 2, Fig. 4, fraction A).

*2.8.3.2. 13^2(R)-Hydroxychlorophyll a (**4**).* ^{1}H NMR (acetone-d_6), δ_H [ppm]: 9.78 (s, 10-CH), 9.46 (s, 5-CH), 8.61 (s, 20-CH), 8.14 (dd, $^3J_{cis}$ = 11.6 Hz, $^3J_{trans}$ = 17.9 Hz, 3^1-CH), 6.22 (dd, $^2J_{gem}$ = 1.8 Hz, $^3J_{trans}$ = 17.9 Hz, 3^2-CH_2, H_{trans}), 6.02 (dd, $^2J_{gem}$ = 1.8 Hz, $^3J_{cis}$ = 11.6 Hz, 3^2-CH_2, H_{cis}), 6.02 (s, 13^2-COH), 5.14 (tq, $^3J_{P2-P1}$ = 7.2 Hz, $^4J_{P2-P3^1}$ = 1.2 Hz, P2-CH), 4.70—4.64 (m, 17-CH), 4.55 (q, $^3J_{18-18^1}$ = 7.2 Hz, 18-CH), 4.44 (d, $^3J_{P2-P1}$ = 7.2 Hz, P1-CH_2), 3.83 (q, $^3J_{8^1-8^2}$ = 7.6 Hz, 8^1-CH_2), 3.64 (s, 12^1-CH_3), 3.60 (s, 13^4-CH_3), 3.36 (s, 2^1-CH_3), 3.31 (s, 7^1-CH_3), 2.90—2.08 (m, 17^1-CH_2, 17^2-CH_2)[a], 1.96—1.82 (m, P4-CH_2)[b], 1.71 (t, $^3J_{8^2-8^1}$ = 7.6 Hz, 8^2-CH_3), 1.65 (d, $^3J_{18^1-18}$ = 7.2 Hz, 18^1-CH_3), and 1.56 (d, $^4J_{P2-P3^1}$ = 1.2 Hz, P3^1-CH_3); [a]Needs spin simulation for the fragment 17-CH–17^1-CH^2–17^2-CH_2; [b]The assignments of the phytyl P5–P16 proton signals were similar to those reported elsewhere [79]. $^{13}C\{^1H\}$ NMR (acetone-d_6), δ_C [ppm]: 193.41 (13^1), 173.91 (17^3), 170.51 (19), 162.88 (14), 157.96 (16), 156.03 (1), 153.02 (6), 147.32 (9), 149.23 (4), 148.76 (11), 145.40 (8), 143.15 (P3), 140.40 (3), 135.20 (7), 136.56 (2), 135.48 (12), 131.77 (3^1), 129.74 (13), 120.62 (3^2), 119.64 (P2), 109.72 (15), 108.45 (10), 101.28 (5), 94.34 (20), 91.14 (13^2), 61.56 (P1), 50.51 (17), 50.39 (18), 40.40 (P4), ~31.07 (17^1), ~31.07 (17^2), 23.45 (18^1), 20.02 (8^1), 18.07 (8^2), 16.24 (P3^1), 12.78 (12^1), 12.58 (2^1), and 11.17 (7^1); the assignments of the phytyl P5–P16 carbon signals were similar to those reported elsewhere [79]. FAB-MS: *m/z* 908.4 [$M^{+\cdot}$]; $C_{55}H_{72}N_4O_6Mg$ requires 908.5. UV–vis in Et_2O: λ_{max} (relative intensity) at 661.6 (0.847), 614.5 (0.139), 573.5 (0.076), 530.3 (0.043), 429.3 (1.000) and 410.9sh, (0.761) nm (Table 2, Fig. 4, fraction A).

3. Results

3.1. Progress of the HRP-catalyzed reaction

Under the optimal reaction conditions ([H_2O_2] = 491 μM, [Chl *a*] = 38 μM, [HRP] = 1.0 μM, in potassium phosphate buffer, 0.1 M, pH 5.9,

Table 2
Electronic absorption spectra in Et_2O of the fractions A–F in Fig. 3.

Fraction	V_m [mL]	Absorption maxima, λ_{max} [nm] (relative intensity)
A	240–294	660 (0.78), 612 (0.11), 570 (0.057), 526 (0.039), 427 (1.00), 410 (0.68), 380 (0.39)
B	358–456	650 (0.50), 604 (0.078), 562 (0.042), 519 (0.033), 417 (1.00)
C	478–512	682sh (0.43), 654 (0.39), 610 (0.11), 525 (0.079), 450sh (0.24), 416 (1.00)
D	530–553	680sh (0.15), 660 (0.29), 613 (0.075), 537 (0.32), 505 (0.28), 454sh (0.59), 422 (1.00)
E	555–565	660 (0.46), 613 (0.10), 572 (0.067), 530 (0.067), 421 (1.00)
F	604–610	686sh (0.12), 656 (0.37), 610 (0.13), 537 (0.28), 505 (0.25), 455sh (0.48), 420 (1.00)

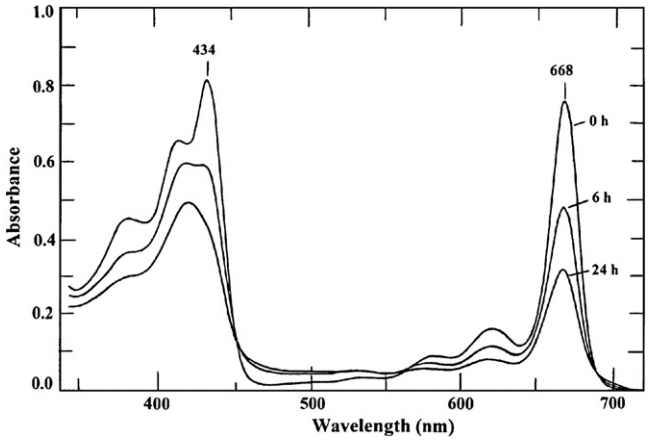

Fig. 2. Kinetics of the HRP-catalyzed reaction of Triton X-100 solubilized Chl *a*.

containing 0.25% of Triton X-100), the reaction proceeded smoothly. This was indicated by the noticeable changes occurring in the electronic absorption spectrum (UV–vis), recorded from aliquots taken from the reaction mixture at 0 h, 6 h, and 24 h (Fig. 2). In the course of the reaction, the intensity of the chlorin band (λ_{max} at 668 nm, 0 h) and that of the Soret band (λ_{max} at 434 nm, 0 h) diminished markedly and also the form and position of the Soret band changed (λ_{max} at 420 nm, 24 h). In contrast, the absorbance increased slightly in the region of 450–560 nm (Fig. 2). Noteworthy is that the UV–vis spectrum at 0 h is closely similar to that of monomeric Chl *a* in diethyl ether or acetone. This indicates that there were no Chl self-aggregates or water-linked Chl aggregates present in the reaction mixture at the beginning of the reaction.

After 24 h, the reaction mixture was transferred into a separatory funnel and the reaction products were extracted into diethyl ether. The transfer of the Triton X-100 micelles, containing the residual Chl and the reaction products, into the Et_2O phase, was promoted by adding sodium chloride to the aqueous phosphate buffer phase. The Et_2O was evaporated from the extract in a rotary evaporator at reduced pressure and ice-cold acetone was added to the residue to disintegrate the detergent-pigment complexes. The mixture, containing ca. 20 mg of pigments/mL, was transferred to the top of the adsorbent layer in a silica gel column (i.d. 2.5 cm, height 50 cm), and the pigments were eluted off the column with cold acetone.

The TLC densitogram recorded from the detergent-free reaction products was compared with that of a mixture, which contained Pheo *a* (Fig. 1, **9**) Chl *a* (**1**), Chl *a*′ (**2**), and $13^2(S/R)$-HO-Chl *a* (**3**/**4**) standards from our collection. Approximately two-thirds of the original amount of Chl *a* had been converted into green oxidized Chl derivatives and some red component(s). The relative mobility (R_p = the distance migrated by the component divided by the distance migrated by Pheo *a*) of the major product (R_p = 0.30) was virtually the same as that of $13^2(S/R)$-HO-Chl *a* (R_p = 0.27) [76]. On the TLC plate, there could be observed also a red component, which moved slower than the standard $13^2(S/R)$-HO-Chl *a*.

To verify that HRP catalyzed the observed reactions of Chl *a*, the following blank tests were performed (for further details, see part 2.5): Chl *a* was incubated with HRP when H_2O_2 was absent and, in another case, with H_2O_2 when HRP was absent. In both blank tests, there was only negligible change in the absorption spectrum of Chl *a*. The TLC, run from the detergent-free products of the blank tests, revealed in both cases the presence of only a small amount of Pheo *a* in addition to the main component, Chl *a*. Accordingly, it was obvious that both HRP and H_2O_2 were necessary and that a real HRP-catalyzed reaction was concerned. This result is in agreement with that by Huff [36].

3.2. Preparative separation of the reaction products on a sucrose column

Soon after beginning the separation with 1% 2-PrOH in LP as eluent, it was observed that a narrow band moved faster than the rest of the sample. After a while, this fast moving band was divided into three components, which emerged from the column partially separated and were identified from the effluent as Pheo *a*′/*a* and Chl *a*′/*a* on the basis of UV–vis spectra and relative mobilities on a sucrose TLC plate [76]. These components also reacted positively to the Molisch phase-test [66–68]. The first oxidation product A, migrated clearly slower than Chl *a* and emerged from the column at V_m = 240–294 mL (Fig. 3, left-hand scale). Overlapping with the tail of fraction A, there followed a blue–green fraction B (V_m = 358–456 mL) (Fig. 3, right-hand scale). At V_m = 380 mL, the eluent polarity was increased by replacing the 1% 2-PrOH in LP with 3% 2-PrOH in LP and then, at V_m = 440 mL, with 5% 2-PrOH in LP. In the tail of fraction B, there appeared fraction C (V_m = 478–512 mL), which was immediately followed by a red zone (fraction D, V_m = 530–553 mL). Fractions E (V_m = 555–565 mL) and F (V_m = 604–610 mL) emerged last from the column. The colour of E was bright green and that of F was again red.

3.3. Characterization of the reaction products A–F

The electronic absorption spectrum of fraction A was practically identical with that of Chl *a* (Table 2, Fig. 4). The spectrum of fraction B (Table 2, Fig. 4) was identical with that of the Mg-$15^1(S/R)$-HO-lactone derivative, that is, the 15^2-methyl, 17^3-phytyl ester of Mg-unstable chlorin [Mg-3^1,3^2-didehydro-15^1,15^1-dihydroxy-rhodochlorin-15-acetic acid $15^1(S/R)$-δ-lactone] (Fig. 6, **14**/**15**) [68,80]. The identity of component B with the lactone **14** or **15** was verified by

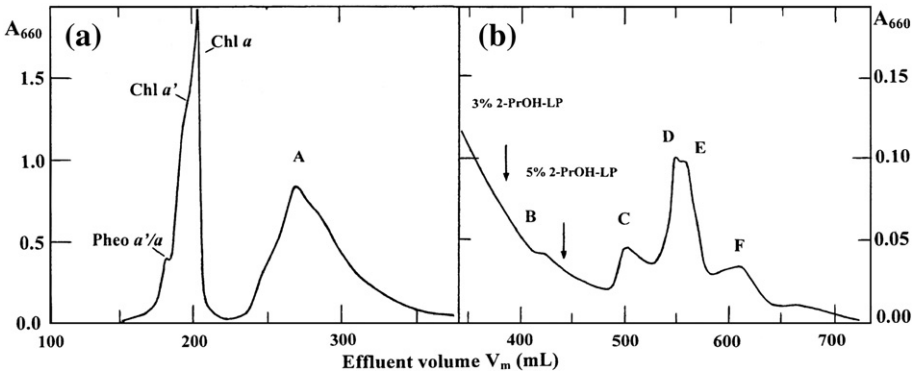

Fig. 3. The elution profile of the preparative separation of the reaction products on a sucrose column.

the following properties: (1) The UV–vis spectrum of B was identical with that of the Mg-15^1(*R*/*S*)-methoxy-lactone allomers of Chl *a*, the structures of which have been established by completely assigned ^{1}H and ^{13}C NMR spectra [79,81,82]. (2) The formation of the Mg-15^1(*S*/*R*)-HO-lactone allomers is expected under the conditions of this work where water was as solvent instead of methanol. (3) Diazomethane converted B to the 13^1,15^2-dimethyl, 17^3-phytyl ester of Mg-purpurin 7 (**18**) [Mg-3^1,3^2-didehydro-rhodochlorin-15-glyoxylic acid] [68,80]. The structure of compound **18** has been established by its UV–vis spectrum [68,83] and the ^{1}H and ^{13}C NMR spectra [81,82]. (4) The relative mobility (R_p) of B in sucrose TLC was 0.27, which is in harmony with the presence of a hydroxyl group in the molecule and also is quite close to the R_p value of 0.21, reported for this Chl derivative [76].

The UV–vis spectrum of fraction C was similar to that of B as to the positions of the chlorin band at 654 nm and the Soret band at 416 nm (Table 2, Fig. 4). Hence, fraction C possibly contained the other diastereomer of B. However, it is also possible that peak C resulted at least partly from the accumulation of the tail of B as a consequence of increasing the concentration of 2-PrOH in the eluent. There are three possible factors that account for the shoulders (sh) in the spectrum of C: (1) self-aggregation; (2) overlapping of C by fractions D and E, as the resolution among the three was quite incomplete; (3) demethylation of the 15^1-methoxycarbonyl group of B to a carboxyl group and conversion of the 15^1-diastereomeric products to the 17^3-phytyl ester of Mg-purpurin-18 [Mg-3^1,3^2-didehydro-15-carboxy-rhodochlorin anhydride] (Fig. 6, **19**) [68,84], which is formed easily from the Mg-15^1(*S*/*R*)-HO-lactone derivatives (Fig. 6, **14**/**15**) [66,85]. Each of the fractions A–C reacted negatively to the Molisch phase-test [66–68]. The spectrum of E (Table 2, Fig. 5) resembled that of B by form, but showed bathochromic shifts for the positions of the absorption maxima, which are in a better agreement with the spectral properties of A than with those of B. In addition, the spectrum, taken from a fraction (V_m = 581–595 mL) between peaks E and F, resembled closely that of E regarding the positions of the maxima but exhibited a clearly broader Soret band. Therefore, we see as possible candidates for E, a Chl *a* derivative, carrying a carboxyl group and a hydroxyl, hydroperoxyl or hydroperoxide anion group at C-13^2, overlapped presumably by the 17^3-phytyl ester of Mg-unstable chlorin 7 with a free carboxyl group at 15^1 instead of a methoxycarbonyl (Fig. 6, **16**/**17**) [68,85]. The very low mobility of E

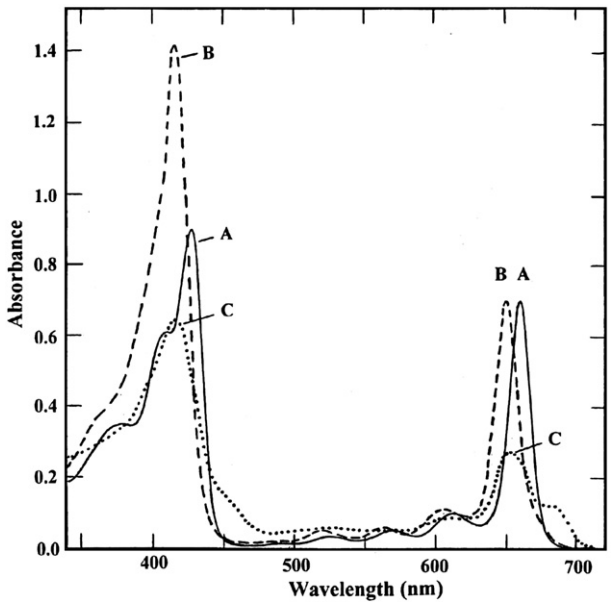

Fig. 4. Electronic absorption spectra of fractions A, B, and C in Fig. 3.

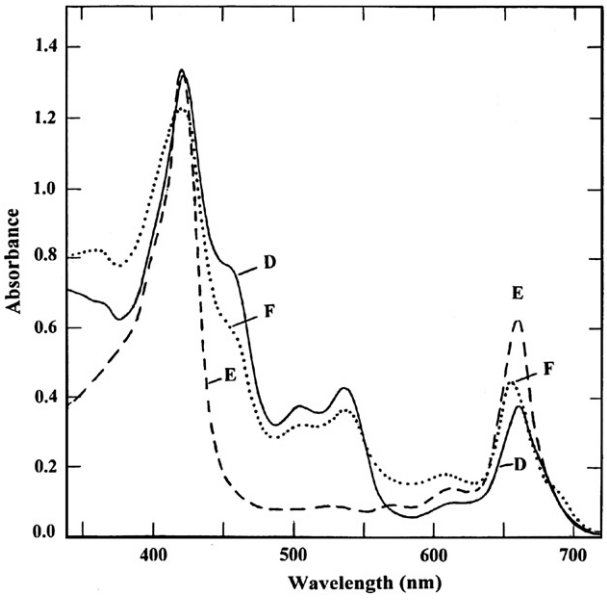

Fig. 5. Electronic absorption spectra of fractions D, E, and F in Fig. 3.

(R_p = 0.12) in sucrose TLC is in harmony with the presence of very polar functional groups in the molecule.

Particularly interesting are the absorption spectra of fractions D and F, which are unique in showing relatively high-intensity absorption bands in the region of 450–570 nm and low-intensity bands in the

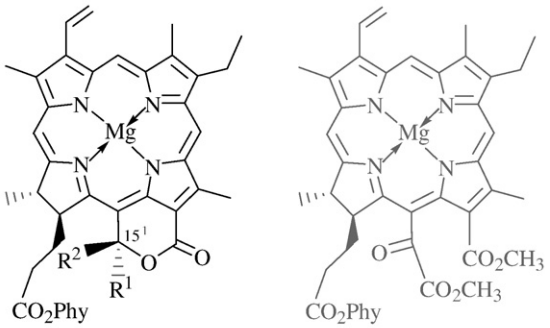

14 R^1=CO$_2$CH$_3$; R^2=OH;
15 R^1=OH; R^2=CO$_2$CH$_3$;
16 R^1=CO$_2$H; R^2=OH;
17 R^1=OH; R^2=CO$_2$H

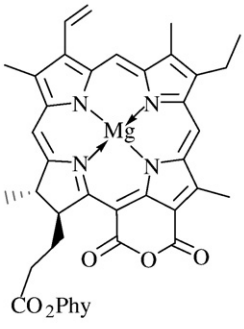

Fig. 6. Structures of the phytyl esters of the Mg-15^1(*S*/*R*)-HO-lactone derivatives (**14–17**), the 13^1,15^2-dimethyl, 17^3-phytyl ester of purpurin 7 (**18**), and the 17^3-phytyl ester of Mg-purpurin 18 (**19**).

chlorin band region, 640–750 nm. Such spectra are typical of the so-called phase-test intermediate, PTI [66–73], which has been characterized by ^{1}H NMR as the enolate anion of Chl [72,73]. In pure state, the enolate anion of Chl *a* or *b* exhibits in pyridine solution a colour of red-wine which is in line with the distinct changes in the absorption spectrum as compared with the original Chl. We have recently prepared the enolate anion of each Chl in pyridine solution under strictly inert conditions (argon atmosphere) using a sterically hindered base, such as *tert*-butoxide (this is a strong base but a weak nucleophile) to deprotonate completely the 13^2-CH group of Chl (this reaction results in the Chl enolate resonance hybrid, see Scheme 4) but to avoid the nucleophilic attack of the base to the 13^1-C=O carbon (this reaction would open the isocyclic ring E). Fig. 7 shows the UV–vis spectrum of Chl *a* enolate, prepared by us under the inert conditions.

This spectrum is closely similar to the PTI spectrum reported by Seely (see Fig. 1 in reference [66]), except that in our spectrum the two bands at 375 and 424 nm show higher intensities than those in the spectrum of Seely. The UV–vis spectrum of the Pheo *a* enolate/methyl Pheide *a* enolate ion is similar to that of the Chl *a* enolate ion in the region between 450 and 750 nm but shows a uniform band at 375 nm [66,70].

Comparison of the Chl *a* enolate ion spectrum in Fig. 7 with the spectra of components D and F in Fig. 5 shows close similarity of the bands in the range of 480–580 nm. In addition, the splitting of absorption in the Soret band region (350–480 nm, Fig. 7) is indicated by a shoulder at 470 nm in the spectra of D and F (Fig. 5). Also, the splitting of absorption in the chlorin band region (630–750 nm, Fig. 7) is indicated by a shoulder at 680 nm, especially in the spectrum of F (Fig. 5). The differences between the enolate spectrum of Fig. 7 and the spectra D and F of Fig. 5 are probably due to overlapping by the spectrum of the chlorin derivative E (Fig. 5). Further, it is noteworthy that the spectra in Figs. 5 and 7 do not match the spectrum of bilirubin (λ_{max} at 450 nm in chloroform [86]) or biliverdin (λ_{max} at 380 and 666 nm in chloroform/methanol, 1:1 [87]).

Consequently, we find as the most likely candidates for E and F the enolate anions of Pheo *a* and Chl *a* or, alternatively, two different complexes of the Chl *a* enolate ion with the detergent molecules (this alternative is based on the assumption that the polar enolate ion of Chl was bound firmly with the detergent molecules, which were not completely stripped off in the removal procedure, see part 2.6). It was not possible to apply more powerful spectrometric methods to the structural characterization of the components in fractions C–F because of their small amounts, instability, and incomplete separation from one another. However, the main reaction product, fraction A, was subjected to a more thorough purification, followed by structure determination using NMR and MS.

In the re-purification of fraction A, the chromatographic procedures on a new silica gel column and a new sucrose column were repeated. When the re-purified sample was analyzed by sucrose TLC, applying three successive developments with 1% 2-PrOH in LP, a complete resolution between the 13^2(*S*) and 13^2(*R*)-HO-Chl *a* diastereomers was achieved (Fig. 8). Integration of the peaks in the densitogram gave an *S*:*R* ratio of 1:2.3. The NMR spectroscopic analysis of the diastereomers provided ^{1}H and ^{13}C chemical shift data (see parts 2.8.3.1 and 2.8.3.2), which are practically identical with our published data for these diastereomers [75,80,82]. The mass spectrometric results confirmed that the diastereomers were hydroxychlorophylls.

Among the ^{1}H chemical shift data, the δ_H-values, 6.05 and 6.02, belonging to the 13^2-COH proton of 13^2(*S*)-HO-Chl *a* and 13^2(*R*)-HO-Chl *a*, deserve special attention, because these values are very close to the δ_H-values, 6.15 and 6.04, of 13^2(*R*)-Chl *a* and 13^2(*S*)-Chl *a* [77,88]. Therefore, it would be very difficult to distinguish the 13^2-hydroxylated chlorophylls from the intact, naturally occurring chlorophylls solely on the basis of the ^{1}H NMR and UV–vis spectra [the UV–vis spectra are identical for 13^2(*S*/*R*)-HO-Chl *a* and 13^2(*S*/*R*)-Chl *a*].

Inspection of the differences in the δ_C-values between the 13^2(*S*) and 13^2(*R*) diasteomers of 13^2-HO-Chl *a* indicates that the change of configuration at C-13^2 induces only slight differences in the ^{13}C chemical shifts. Of special interest are the δ_C-values of C-13^2, which are at ca. 91 ppm for both diastereomers of 13^2-HO-Chl *a*. This carbon is deshielded by ca. 25 ppm relative to the C-13^2 of 13^2(*R*)-Chl *a* (δ_C = 65.5) [75,80,82]. Owing to this, ^{13}C NMR spectroscopy is a good method to distinguish the 13^2-hydroxylated chlorophylls from the intact, naturally occurring chlorophylls.

4. Discussion

The foregoing results showed that, in the absence of a phenol, the HRP-catalyzed reaction of the detergent-solubilized Chl *a* with H_2O_2 produced the 13^2(*S*) and 13^2(*R*) diastereomers of 13^2-HO-Chl *a* (*S*:

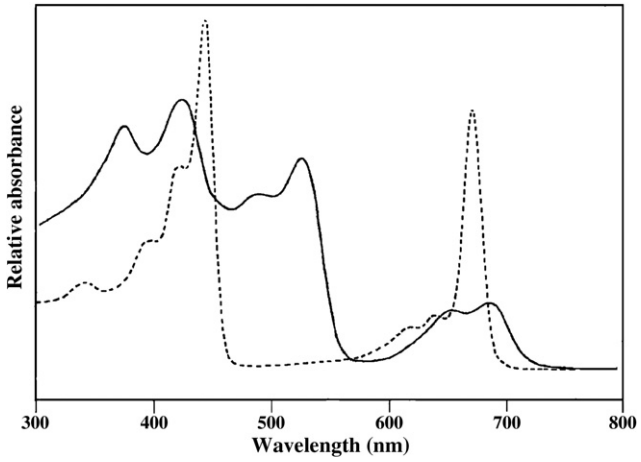

Fig. 7. Electronic absorption spectra of Chl *a*, **1** (···) and its enolate anion (—) (Scheme 4) in pyridine. To prepare the enolate anion, an amount of 0.5 mg of potassium *tert*-butoxide was added to a pyridine solution (3.0 mL) of Chl *a*, $c = 2.03 \times 10^{-5}$ mol L^{-1}, in a quartz cuvette (light path = 10 mm). The solution was deoxygenated by bubbling argon gas through it before and during the addition of the base and the cuvette was closed air-tight with a Teflon stopper.

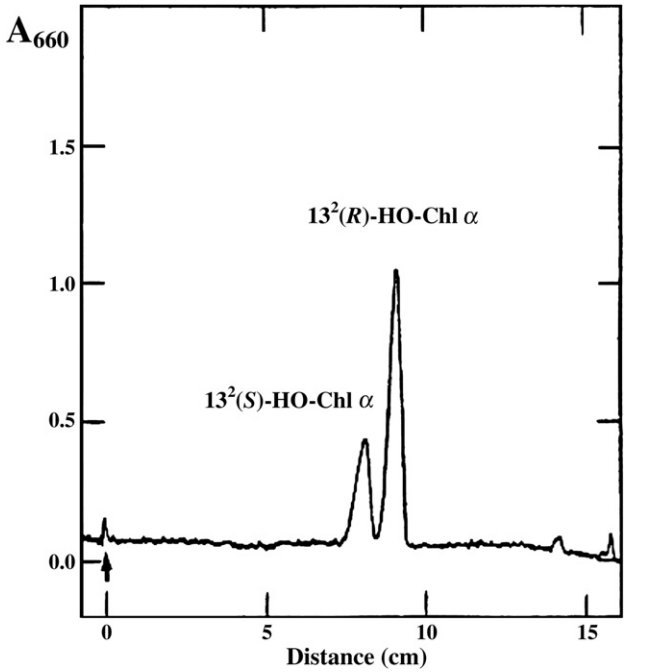

Fig. 8. Resolution of the 13^2-HO-Chl *a* diastereomers (epimers) by sucrose TLC applying three successive developments with 1% 2-PrOH in LP.

$R = 1{:}2.3$) as the main oxidation products. Hence, the 'Chl oxidase' of Schoch et al. [46] could well be a peroxidase enzyme. Under our reaction conditions, the HRP catalysis also yielded the 15^2-methyl, 17^3-phytyl ester of Mg-unstable chlorin from Chl *a*, as well as two red components, which probably represent the enolate ions of Pheo *a* and Chl *a* or, alternatively, two different complexes of the Chl *a* enolate ion with the detergent molecules. Distinctly, the red components are not the 'bilirubin-like pigments', proposed by several researchers [51,52,54].

Consequently, our results are fully consistent with the free-radical allomerization (FRA) mechanism [70,89–91], considering that, in the present case, we have water instead of methanol. In this mechanism, a key intermediate is the Chl enolate ion, which is a resonance hybrid, produced by deprotonation of the Chl 13^2-CH group (vide infra, Scheme 4). The Chl enolate ion is highly reactive with ground-state (triplet) oxygen, $^3O_2$, $^3\Sigma_g^-$, thereby yielding the Chl 13^2-C• radical and the superoxide anion radical, $O_2^{-\bullet}$. The FRA reaction scheme then continues as reported previously [70,89–91]. Apparently, the presence of HRP and H_2O_2 in the reaction mixture accelerated the rate of the allomerization reaction of Chl. The blank tests performed (see part 2.5) verified that both HRP and H_2O_2 were needed to bring about this acceleration effect. Under these circumstances, an interesting question follows: What was the exact molecular mechanism of the action of HRP and H_2O_2 to bring about the acceleration of the FRA reaction of Chl?

To understand better the mechanism of the HRP catalysis in the present case, we have to remember that we used Triton X-100 to solubilize Chl *a* in the aqueous buffer solution, because Chl *a* is entirely insoluble in water. Therefore, we need to consider how the non-ionic molecules of Triton X-100 (*t*-octylphenoxypolyethoxyethanol) are organized in the micelles formed in aqueous solutions and how the Chl *a* molecules orientate themselves in these micelles [65,92,93]. We can assume that, in spherical micelles, the Triton X-100 molecules would orientate themselves so that the non-polar *t*-octylphenyl groups form the hydrophobic core of the micelle while the polar polyethoxyethanol groups are directed towards the surface of the micelle, forming hydrogen bonds with water. In such a micelle, the Chl *a* molecule can be envisaged to orientate itself in such a fashion that the long non-polar phytyl group, $C_{20}H_{39}$, is directed towards the hydrophobic core of the micelle, whereas the polar carbonyl groups of the Chl isocyclic ring E are located in the vicinity of the surface of the micelle, or possibly even penetrate out from the surface to enable hydrogen bonding with water [65]. In addition, it should be noted that the behaviour of Chl molecules in a micelle depends on the Chl concentration relative to the detergent concentration, because Chl can form self-aggregates or water-linked aggregates at high Chl concentrations [65]. Inspection of the electronic spectrum of the micellar Chl *a* at the beginning of the HRP reaction (spectrum at 0 h in Fig. 2) indicates the presence of only Chl *a* monomers; there are no signs of the presence of its self-aggregates or water-linked aggregates.

If we assume that the isocyclic ring E of the Chl macrocycle is located in the vicinity of the surface of the detergent micelle and that the access channel on the distal side of the heme coenzyme of HRP is adequately wide and open, then a direct reaction between the Chl and HRP-I or HRP-II, is possible. Under such circumstances, we can replace the reducing substrate RH with Chl, having a labile hydrogen atom at C-13^2, and the free-radical product R• with Chl 13^2-C• radical (see the HRP reaction mechanism in part 1). In this case, a contact between the Chl 13^2-C• and $^3O_2$ or HO• would be possible as well, thus enabling the FRA reaction to proceed as previously proposed [70,89–91].

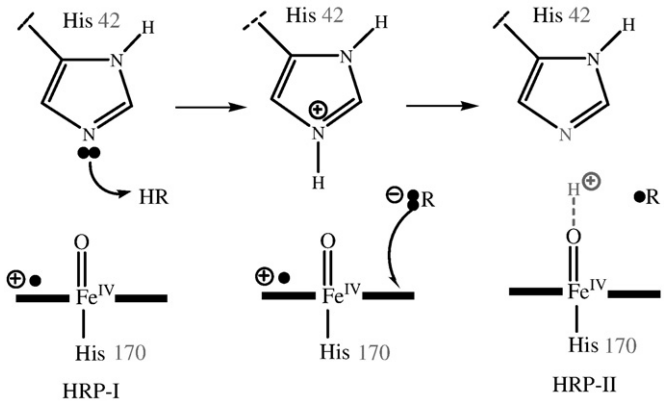

Scheme 3. Plausible mechanism for the reduction of HRP-I to HRP-II in the active centre of HRP [2,24,25]. In our case, the reducing substrate, RH is Chl *a*, its C-13^2 deprotonated form, R:$^-$, is the C-13^2 carbanion limiting structure of the Chl *a* enolate resonance hybrid (Scheme 4), which is oxidized into radical R• , i.e. the C-13^2 radical of Chl *a*, via ejection of one electron.

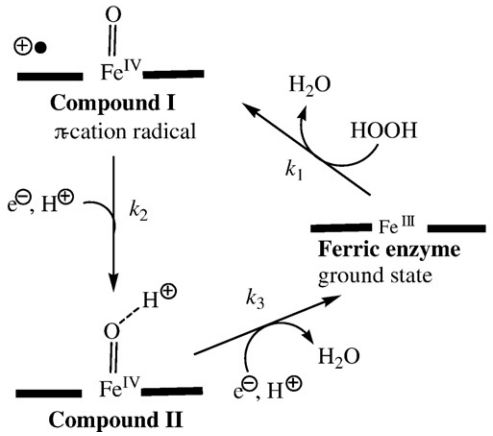

Scheme 2. Peroxidase mechanism in triangle form [26,27]. The proton and electron ($H^{\oplus} + e^{\ominus} = H\bullet$) are provided by the reducing substrate RH, which is converted to the free-radical R• via deprotonation followed by electron transfer.

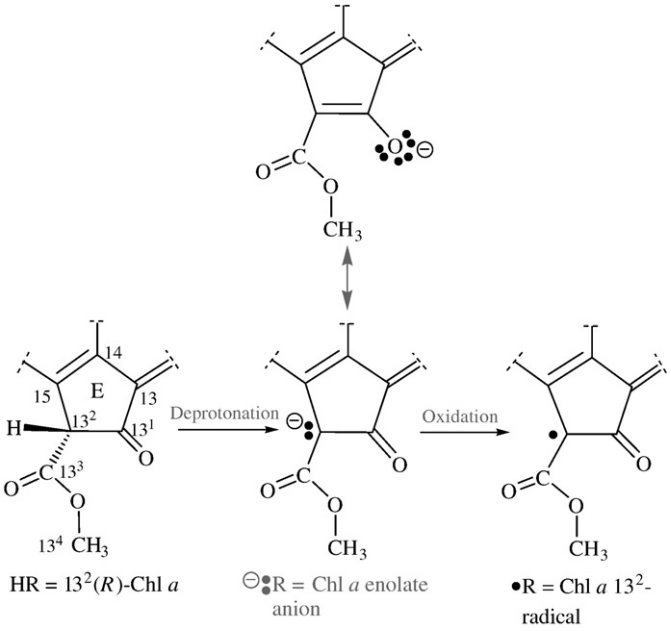

Scheme 4. Reactions undergone by $13^2(R)$-Chl *a* in the active centre of HRP while HRP-I is reduced to HRP-II (reaction (2)) and HRP-II to the ferric ground-state (reaction (3)). The double-headed arrow denotes mesomerism (resonance).

Nevertheless, we should also consider a situation where the macrocycle of Chl is located deeper in the detergent micelle but close to the polyethoxy chain of the Triton X-100 molecule. As this chain contains several autoxidizable ethoxy groups with ethereal linkages and because the relatively small triplet dioxygen, $^3O_2$, would be expected to be capable of diffusing into the detergent micelle, the production superoxide anion radicals, $O_2^{-\bullet}$, is possible as a result of the autoxidation [94]. The $O_2^{-\bullet}$ probably is capable of abstracting a H• atom, i.e. a proton and electron from the Chl 13^2-CH group, producing a Chl 13^2-C• radical, which would continue the free-radical chain reaction according to the reported reaction scheme [70,89–91]. However, under such circumstances, the catalytic effect of the HRP enzyme, which was verified by the blank tests, should also be accounted for in further detail. Apparently, to cause the catalytic effect of HRP would demand that the detergent's terminal ethanol HO-group and/or the ethoxy CH_2-groups are located adequately close to the surface of the micelle and the isocyclic ring of the Chl macrocycle. Such an arrangement would enable these groups to act as reducing substrate for HRP-I and HRP-II, thereby producing free-radical species to initiate the FRA of Chl.

The HRP-catalyzed oxidation of the detergent-solubilized Chl with H_2O_2 is made even more complicated by the experimental observation that the reaction produced two red components, interpreted as representing the enolate ions of Pheo *a* and Chl *a* or two different complexes of the Chl *a* enolate ion with Triton X-100. This conspicuous experimental observation deserves special attention, because it is the first time that such red Chl derivatives were observed on a chromatography column. The possibility that the enolates were produced as a result of base impurities, present in the materials of the HRP reaction or the chromatographic system, is unlikely, considering the results of the blank tests and the initial spectrum of Chl in Fig. 2. It seems more likely that the formation of the enolates is associated with the mechanism inherent in the HRP catalysis. Hence, in an attempt to find a reasonable explanation for the conspicuous experimental result, we have to deepen our insight into the mechanism of the HRP-catalyzed reaction.

In addition to the reactions (1)–(3), shown in part 1, it is illustrative to present the peroxidase cycle in a triangle form, which shows the movement of protons and electrons (Scheme 2) [26,27].

According to Scheme 2, the reduction of HRP-I to HRP-II and of HRP-II to the ferric ground-state of the HRP enzyme consists of two steps: deprotonation of the reducing substrate, i.e. proton abstraction from the substrate, followed by electron transfer. It has been reported that the electron transfer step in the reduction of HRP-I to HRP-II is the rate-determining step in the HRP catalytic cycle [2,24,25]. This implies in our case, where Chl *a* is the reducing substrate RH, that the deprotonation of the Chl 13^2-CH group, which yields the Chl enolate ion, takes place more rapidly than the oxidation of the enolate ion to the Chl 13^2-radical (Scheme 3). To make it clear, the two reactions occurring to Chl *a* are shown in Scheme 4 (Chl *a*′, i.e. $13^2(S)$-Chl *a*, reacts likewise).

Chl *a*/*a*′ undergoes the same reactions also in reaction step (3) of the peroxidase catalytic cycle, where HRP-II is reduced to the original ferric state of HRP (Scheme 2). In this connection, it is important to understand that the Chl enolate ion must be regarded as a resonance hybrid whose electronic structure can only be described in terms of limiting Lewis structures (contributors). Scheme 4 shows only two main contributors, the 13^2-carbanion structure and the 13^1-oxyanion, for the Chl enolate ion resonance hybrid. Though these are the principal contributors to the electronic structure of the Chl enolate ion, comparable with those usually written for organic enolate ions, they are not adequate to describe the precise electronic structure of the Chl enolate ion, because the negative charge is partially delocalized over the macrocyclic π-system. The limiting structure with the negative charge on the nitrogen of the 'pyrrolenine' ring B was considered by Seely [66] to have a substantial contribution in the resonance hybrid on the basis of Woodward's assumption [95] that the pyrrolenine ring B tends to attract electrons more strongly than the sub-rings A, C, or D [66,70]. This structure shows an interrupted delocalized π-system, which seems to explain the profound alterations in the electronic spectrum of the enolate ion (Fig. 7). In addition, it is noteworthy that the mesomerism (resonance) of the enolate ion [66,70,73,80,89] and the possible complex formation between the enolate ion and the polar chains of the Triton X-100 molecules, have stabilizing effects on the enolate ion. These stabilizing effects and the possible depletion of $^3O_2$ inside the sucrose column are expected to retard the reactivity of the enolate ion.

5. Conclusion

The afore-said provides a reasonable explanation for the observed catalytic effect of the HRP reaction cycle on the allomerization of Chl. The same reactive Chl derivatives, i.e. the Chl enolate anion and the Chl 13^2-radical, which are produced twice by the HRP reaction cycle, happen to be the crucial intermediates in the initial stages of the Chl allomerization mechanism [70,89–91]. It is noteworthy that the Chl allomerization, which involves oxidation of Chl in the dark by ground-state, i.e. triplet-state dioxygen, $^3O_2$, $^3\Sigma_g^-$, has never been observed by us to result in bilins, the formation of which would require the oxygenolysis of the chlorin macrocycle. For the oxygenolysis to occur, the HRP should show a dioxygenase or PaO-like monooxygenase activity, which has not been observed. Our result that the HRP-catalyzed oxidation of Chl *a* does not involve the oxygenolysis of the chlorin macrocycle is in line with the results from the investigations by Pont et al. [18] and Jacobs et al. [19]. We emphasize that our experimental procedures were performed in the dark or dimmed light to avoid the formation of singlet-state dioxygen, $^1O_2$, $^1\Delta_g$, via energy transfer from the triplet-state Chl (or its Mg-free derivative) to $^3O_2$, a process known as photosensitization. Unlike $^3O_2$, the $^1O_2$ is capable of cycloadding to a methine bridge of the chlorin macrocycle, resulting in the opening of macrocycle to form a bilin [55,56].

References

[1] B.C. Saunders, A.G. Holmes-Siedle, B.P. Stark, Peroxidase, Butterworths, London, 1964.
[2] H.B. Dunford, Horseradish peroxidase: structure and kinetic properties, in: J. Everse, K.E. Everse, M.B. Grisham (Eds.), Peroxidases in Chemistry and Biology, vol. 2, CRC Press, Boca Raton, FL, 1991, pp. 1–24.
[3] H.B. Dunford, Heme Peroxidases, Wiley-VCH, New York, 1999.
[4] R.P. Ferrari, S. Traversa, Structure function relationship amongst members of animal peroxidase family of proteins, The Peroxidase Multigene Family of Enzymes: Biochemical Basis and Clinical Applications, Springer-Verlag, Berlin, 2000, pp. 114–120.
[5] K.G. Welinder, Plant peroxidases: structure–function relationships, in: C. Penel, T. Gaspar, H. Greppin (Eds.), Plant Peroxidases 1980–1990. Topics and Detailed Literature on Molecular, Biochemical, and Physiological Aspects, University of Geneva, Geneva, 1992, pp. 1–24.
[6] K.G. Welinder, M. Gajhede, Structure and evolution of peroxidases, in: K.G. Welinder, S.K. Rasmussen, C. Penel, H. Greppin (Eds.), Plant Peroxidases: Biochemistry and Physiology, University of Geneva, Geneva, 1993, pp. 35–42.
[7] P.R. Ortiz de Montellano, Catalytic sites of hemoprotein peroxidases, Annu. Rev. Pharmacol. Toxicol. 32 (1992) 89–107.
[8] K.G. Welinder, J.M. Mauro, L. Norskov-Lauritsen, Structure of plant and fungal peroxidases, Biochem. Soc. Trans. 20 (1992) 337–340.
[9] K.G. Welinder, Superfamily of plant, fungal and bacterial peroxidases, Curr. Opin. Struct. Biol. 2 (1992) 388–393.
[10] A.T. Smith, N.C. Veitch, Substrate binding and catalysis in heme peroxidases, Curr. Opin. Chem. Biol. 2 (1998) 269–278.
[11] N.C. Veitch, A.T. Smith, Horseradish peroxidase, Adv. Inorg. Chem. 51 (2001) 107–162.
[12] N.C. Veitch, Structural determinants of plant peroxidase function, Phytochem. Rev. 3 (2004) 3–18.
[13] H.B. Dunford, J.S. Stillman, On the function and mechanism of action of peroxidases, Coord. Chem. Rev. 19 (1976) 187–251.
[14] PROMISE mirror: http://metallo.scripps.edu/promise/FPBPEROXIDASES.html.
[15] S. Ardissone, P. Frendo, E. Laurenti, W. Jantschko, C. Obinger, A. Puppo, R.P. Ferrari, Purification and physical–chemical characterization of the three hydroperoxidases from the symbiotic bacterium *Sinorhizobium meliloti*, Biochemistry 43 (2004) 12692–12699.

[16] S.M. Kapetanaki, S. Chouchane, S. Yu, X. Zhao, R. Magliozzo, P.M. Schelvis, *Mycobacterium tuberculosis* KatG(S315T) catalase-peroxidase retains all active site properties for proper catalytic function, Biochemistry 44 (2005) 243–252.
[17] M.P.J. van Deurzen, F. van Rantwijk, R.A. Sheldon, Selective oxidations catalyzed by peroxidases, Tetrahedron 53 (1997) 13183–13220.
[18] F. Pont, N.J. Jacobs, N.F.-P. Montforts, Formation of chlorins by oxidation of deuteroporphyrin with horseradish peroxidase, Tetrahedron Lett. 38 (1997) 6383–6384.
[19] N.J. Jacobs, H.G. Kruszyna, H.J.S.L. Hier, F.E. Dayan, S.O. Duke, F. Pont, F.-P. Montforts, Glutathione-dependent oxidative modification of protoporphyrin and other dicarboxylic porphyrins by mammalian and plant peroxidases, Biochem. Biophys. Res. Commun. 259 (1999) 195–200.
[20] R. Russ, T. Zelinski, T. Anke, Benzylic biooxidation of various toluenes to aldehydes by peroxidase, Tetrahedron Lett. 43 (2002) 791–793.
[21] D.J. Bougioukou, I. Smonou, Chloroperoxidase-catalyzed oxidation of conjugated dienoic esters, Tetrahedron Lett. 43 (2002) 339–342.
[22] D. Keilin, E.F. Hartree, Purification of horseradish peroxidase and comparison of its properties with those of catalase and methaemoglobin, Biochem. J. 49 (1951) 88–104.
[23] M. Gajhede, D.J. Schuller, D.A. Henriksen, A.T. Smith, A.T.L. Poulos, Crystal structure of horseradish peroxidase C at 2.15 Å resolution, Nature 4 (1997) 1032–1038.
[24] D. Job, H.B. Dunford, Substituent effect on the oxidation of phenols and aromatic amines by horseradish peroxidase compound I, Eur. J. Biochem. 66 (1976) 607–614.
[25] M. Tanaka, K. Ishimori, M. Mukai, T. Kitagawa, I. Morishima, Catalytic activities and structural properties of horseradish peroxidase distal His42→Gln mutant, Biochemistry 36 (1997) 9889–9898.
[26] G.I. Berglund, G.H. Carlsson, A.T. Smith, A.H. Szöke, A. Henriksen, J. Hajdu, The catalytic pathway of horseradish peroxidase at high resolution, Nature 417 (2002) 463–468.
[27] G.H. Carlsson, P. Nicholls, D. Svistunenko, G.I. Berglund, J. Hajdu, Complexes of horseradish peroxidase with formate, acetate, and carbon monoxide, Biochemistry 44 (2005) 635–642.
[28] J.N. Rodriguez-Lopez, D.J. Lowe, J. Hernandez-Ruiz, A.N.P. Hiner, F. Garcia-Canovas, R.N.F. Thorneley, Mechanism of reaction of hydrogen peroxide with horseradish peroxidase: Identification of intermediates in the catalytic cycle, J. Am. Chem. Soc. 123 (2001) 11838–11847.
[29] D. Dolphin, A. Forman, D.C. Borg, J. Fajer, R.H. Felton, Compounds I of catalase and horseradish peroxidase: π-cation radicals, Proc. Natl. Acad. Sci. U. S. A. 68 (1971) 614–618.
[30] C.E. Schultz, P.W. Devaney, H. Winkler, P.G. Debrunner, N. Doan, R. Chiang, R. Rutter, L.P. Hager, Horseradish peroxidase compound I: evidence for spin coupling between heme iron and a 'free' radical, Febs. Lett. 103 (1979) 102–105.
[31] J.E. Roberts, B.M. Hoffman, R. Rutter, L.P. Hager, Electron-nuclear double resonance of horseradish peroxidase compound I, J. Biol. Chem. 256 (1981) 2118–2121.
[32] R. Rutter, M. Valentine, M.P. Hendrish, L.P. Hager, P.G. Debrunner, Chemical nature of porphyrin π-cation radical in horseradish peroxidase compound I, Biochemistry 22 (1983) 4769–4774.
[33] J. Terner, A.J. Sitter, C.M. Reczek, Resonance Raman spectroscopic characterization of horseradish peroxidase. Observation of $Fe^{IV}=O$ stretching vibration of compound II, Biochim. Biophys. Acta 828 (1985) 73–80.
[34] G.N. LaMar, J.S. de Ropp, L. Lato-Grazynski, A.L. Balch, R.B. Johnson, K.M. Smith, D. W. Parish, R.-J. Cheng, Proton NMR characterization in model heme complexes and hemoproteins: evidence for the $Fe^{IV}=O$ group in ferryl myoglobin and compound II of horseradish peroxidase, J. Am. Chem. Soc. 105 (1983) 782–787.
[35] P. Matile, Catabolism of chlorophyll: involvement of a peroxidase? Zeitschr. Pflanzenphysiol. 99 (1980) 475–478.
[36] A. Huff, Peroxidase-catalyzed oxidation of chlorophyll by hydrogen peroxide, Phytochemistry 21 (1982) 261–265.
[37] E. Martinoia, M.J. Dalling, P. Matile, Catabolism of chlorophyll: demonstration of chloroplast-localized peroxidative and oxidative activities, Zeitschr. Pflanzenphysiol. 107 (1982) 269–279.
[38] M. Kato, S. Shimizu, Chlorophyll metabolism in higher plants. VI. Involvement of peroxidase in chlorophyll degradation, Plant Cell Physiol. 26 (1985) 1291–1301.
[39] M. Kato, S. Shimizu, Chlorophyll metabolism in higher plants. VII. Chlorophyll degradation in senescing tobacco leaves: phenolic-dependent peroxidative degradation, Can. J. Bot. 65 (1987) 729–735.
[40] Y. Gong, J.P. Mattheis, Effect of ethylene and 1-methylcyclopropene on chlorophyll catabolism of broccoli florets, Plant Growth Regul. 40 (2003) 33–38.
[41] B. Lüthy, E. Martinoia, P. Matile, Thylakoid-associated chlorophyll oxidase — distinction fom lipoxygenase, Zeitschr. Pflanzenphysiol. 113 (1984) 423–434.
[42] B. Lüthy, P. Matile, H. Thomas, Properties of linolenic acid-dependent chlorophyll oxidation in thylakoid membranes, J. Plant Physiol. 132 (1986) 169–180.
[43] B. Lüthy, H. Thomas, P. Matile, Linolenic acid-dependent chlorophyll oxidase activity: a property of photosystem I and II, J. Plant Physiol. 123 (1986) 203–209.
[44] H. Thomas, B. Lüthy, P. Matile, Leaf senescence in a non-yellowing mutant of *Festuca pratensis* Huds, Planta 164 (1985) 400–405.
[45] H. Thomas, The role of unsaturated fatty acids in senescence, J. Plant Physiol. 123 (1986) 97–105.
[46] S. Schoch, W. Rüdiger, B. Lüthy, P. Matile, 13^2-Hydroxychlorophyll *a*, the first product in the reaction of chlorophyll oxidase, J. Plant Physiol. 115 (1984) 85–89.
[47] M. Holden, Chlorophyll bleaching by legume seeds — lipoxidase activity of leaves, Phytochemistry 9 (1970) 507–512.
[48] G.A.F. Hendry, J.D. Houghton, S.B. Brown, The degradation of chlorophyll — a biological enigma, New Phytol. 107 (1987) 255–302.
[49] S.B. Brown, J.D. Houghton, G.A.F. Hendry, Chlorophyll breakdown, in: H. Scheer (Ed.), Chlorophylls, CRC Press, Boca Raton, FL, 1991, pp. 465–489.
[50] N. Yamauchi, Y. Funamoto, M. Shigyo, Peroxidase-mediated chlorophyll degradation in horticultural crops, Phytochem. Rev. 3 (2004) 221–228.
[51] Y. Suzuki, Y. Shioi, Detection of chlorophyll breakdown products in the senescent leaves of higher plants, Plant Cell Physiol. 40 (1999) 909–915.
[52] Y. Suzuki, K. Tanabe, Y. Shioi, Determination of chemical oxidation products of chlorophyll and porphyrin by high-performance liquid chromatography, J. Chromatogr. A 839 (1999) 85–91.
[53] R. Azuma, Y. Takahashi, H. Kurata, T. Kawano, K. Shimokawa, M. Adachi, Does peroxidase act as a 'Mg-dechelatase'? Plant Peroxidase Newsletter 13 (1999) 145–151 http://www.unige.ch/LABPV/newsletters/news113/n13p145.html.
[54] M. Adachi, X.W. Ma, K. Adachi, H.I. Kurata, R. Azuma, Y. Takahashi, T. Kawano, K. Shimokawa, Y. Yamauchi, Plant Peroxidase Newsletter (14) (1999) 69–77 http://www.unige.ch/LABPV/newsletters/news114/n14p69.html.
[55] A. Gossauer, Catabolism of tetrapyrroles, Chimia 48 (1994) 352–361.
[56] A. Gossauer, N. Engel, Chlorophyll catabolism — structures, mechanisms, conversions, J. Photochem. Photobiol. B Biol. 32 (1996) 141–151.
[57] P. Matile, S. Hörtensteiner, H. Thomas, B. Kräutler, Chlorophyll breakdown in senescent leaves, Plant. Physiol. 112 (1996) 1403–1409.
[58] P. Matile, S. Hörtensteiner, H. Thomas, Chlorophyll degradation, Annu. Rev. Plant Physiol. Plant Mol. Biol. 50 (1999) 67–95.
[59] B. Kräutler, P. Matile, Solving the riddle of chlorophyll breakdown, Acc. Chem. Res. 32 (1999) 35–43.
[60] S. Hörtensteiner, B. Kräutler, Chlorophyll breakdown in oilseed rape, Photosynth. Res. 64 (2000) 137–146.
[61] K. Takamiya, T. Tsuchiya, H. Ohta, Degradation pathway(s) of chlorophyll: what has gene cloning revealed? Trends Plant Sci. 5 (2000) 426–431.
[62] S. Hörtensteiner, Chlorophyll degradation during senescence, Annu. Rev. Plant Biol. 57 (2006) 55–77.
[63] International Union of Pure and Applied Chemistry (IUPAC), International Union of Biochemistry (IUB), in: G.P. Moss (Ed.), Nomenclature of tetrapyrroles, Pure Appl. Chem., 59, 1987, pp. 779–832.
[64] D.C. Borg, J. Fajer, R.H. Felton, D. Dolphin, The π-cation radical of chlorophyll *a*, Proc. Natl. Acad. Sci. U. S. A. 67 (1970) 813–820.
[65] J.-P. Chauvet, R. Santus, E.J. Land, One-electron oxidation of photosynthetic pigments in micelles. Bacteriochlorophyll *a*, chlorophyll *a*, and pheophytin *a*, J. Phys. Chem. 85 (1981) 3449–3456.
[66] G.R. Seely, The structure and chemistry of the functional groups, in: G.R. Seely, L.P. Vernon (Eds.), The Chlorophylls, Academic Press, New York, 1966, pp. 67–109.
[67] A. Weller, The visible absorption spectra of the phase test intermediates of chlorophyll-*a* and -*b*, J. Am. Chem. Soc. 76 (1954) 5819–5821.
[68] A.S. Holt, The phase test intermediate and the allomerization of chlorophyll *a*, Can. J. Biochem. Physiol. 36 (1958) 439–456.
[69] R. Felton, G.M. Sherman, H. Linschitz, Formation of phase test intermediate of chlorophyll by electrolytic reduction, Nature 203 (1964) 637–639.
[70] P.H. Hynninen, Chemistry of chlorophylls: modifications, in: H. Scheer (Ed.), Chlorophylls, CRC Press, Boca Raton, FL, 1991, pp. 145–209.
[71] M.N. Merzlyak, V.A. Kovrighnikh, N.S. Kuprianova, I.B. Afanas'ev, The allomerization of chlorophylls *a* and *b* with superoxide anion, J. Inorg. Biochem. 24 (1985) 239–242.
[72] S. Lötjönen, P.H. Hynninen, Chlorophylls. VII. An ^1H NMR spectroscopic study of the phase-test intermediate of chlorophyll *a*, Acta Chem. Scand. 44 (1990) 235–238.
[73] P.H. Hynninen, J.S. Kavakka, M. Mesilaakso, Electronic structure of the enolate anion of chlorophyll *b*, Tetrahedron Lett. 46 (2005) 1145–1147.
[74] P.H. Hynninen, Chlorophylls. V. Isolation of chlorophylls *a* and *b* using an improved two-phase extraction method followed by a precipitation and a separation on a sucrose column, Acta Chem. Scand. B31 (1977) 829–835.
[75] P.H. Hynninen, K.J. Pitkänen, Oxidation of chlorophyll *a* with selenium dioxide, J. Porphyr. Phthalocyanines 11 (2007) 566–576.
[76] I. Sahlberg, P.H. Hynninen, Thin-layer chromatography of chlorophylls and their derivatives on sucrose layers, J. Chromatogr. 291 (1984) 331–338.
[77] P.H. Hynninen, S. Lötjönen, Large-scale preparation of crystalline (10*S*)-chlorophylls *a* and *b*, Synthesis 9 (1983) 705–708.
[78] R. Kostiainen, K. Hyvärinen, P.H. Hynninen, Fast-atom bombardment mass spectra of the 13^2-epimers of 13^2-hydroxychlorophyll *a*, Rapid Commun. Mass Spectrom. 9 (1995) 555–558.
[79] I. Kilpeläinen, S. Kaltia, P. Kuronen, K. Hyvärinen, P.H. Hynninen, Assignment of the ^1H and ^{13}C NMR spectra of $13^2(R)$-methoxychlorophyll *a* using the two-dimensional HMQC and HMBC techniques, Magn. Reson. Chem. 32 (1994) 29–35.
[80] P.H. Hynninen, T.S. Leppäkases, M. Mesilaakso, The enolate anions of chlorophylls *a* and *b* as ambident nucleophiles in oxidations with (−)- or (+)-(10-camphorsulfonyl)oxaziridine. Synthesis of $13^2(S/R)$-hydroxychlorophylls *a* and *b*, Tetrahedron 62 (2006) 3412–3422.
[81] P. Kuronen, K. Hyvärinen, I. Kilpeläinen, P.H. Hynninen, High-performance liquid chromatographic separation of the methanolic allomerization products of chlorophyll *a*, J. Chromatogr. A 654 (1993) 93–104.
[82] K. Hyvärinen, J. Helaja, P. Kuronen, I. Kilpeläinen, P.H. Hynninen, ^1H and ^{13}C NMR spectra of the methanolic allomerization products of $13^2(R)$-chlorophyll *a*, Magn. Reson. Chem. 33 (1995) 646–656.
[83] P.H. Hynninen, M.R. Wasielewski, J.J. Katz, Chlorophylls. VI. Epimerization and enolization of chlorophyll *a* and its magnesium-free derivatives, Acta Chem. Scand. B, 33, 1979, pp. 637–648.
[84] P.H. Hynninen, T.S. Leppäkases, M. Mesilaakso, Demethoxycarbonylation and oxidation of $13^2(S/R)$-hydroxychlorophyll *a* to 13^2-demethoxycarbonyl-13^2-oxo-chlorophyll *a* and Mg-purpurin-18 phytyl ester, Tetrahedron. Lett. 47 (2006) 1663–1668.

[85] P.H. Hynninen, S. Assandri, Chlorophylls. II. Allomerization of chlorophylls *a* and *b*, Acta Chem. Scand. 27 (1973) 1478–1486.
[86] H. Du, R.A. Fuh, J. Li, A. Corkan, J.S. Lindsey, PhotochemCAD: A computer-aided design and research tool in photochemistry, Photochem. Photobiol. 68 (1998) 141–142 http://omlc.ogi.edu/spectra/PhotochemCAD/html/bilirubin.html.
[87] A.F. McDonagh, L.A. Palma, Preparation of crystalline biliverdin IXα, Biochem. J. 189 (1980) 193–208.
[88] P.H. Hynninen, S. Lötjönen, Steric interaction between the peripheral substituents of 10(*S*) chlorophyll derivatives and its conformational consequences. A proton magnetic resonance study, Org. Magn. Reson. Chem. 23 (1985) 605–615.
[89] P.H. Hynninen, Mechanism of the allomerization of chlorophyll. Inhibition of the allomerization by carotenoid pigments, Z. Naturforsch. 36b (1981) 1010–1016.
[90] K. Hyvärinen, P.H. Hynninen, Recent developments in the research of the chlorophyll allomerization mechanism, Res. Adv. Org. Bioorg. Chem. 1 (2001) 1–19.
[91] P.H. Hynninen, K. Hyvärinen, Tracing the allomerization pathways of chlorophylls by ^{18}O-labeling and mass spectrometry, J. Org. Chem. 67 (2002) 4055–4061.
[92] R.J. Robson, E.A. Dennis, The size, shape, and hydration of nonionic micelles. Triton X-100, J. Phys. Chem. 81 (1977) 1075–1078.
[93] T. Mukherjee, A.V. Sapre, J.P. Mittal, On the nature of chlorophyll *a* in aqueous micellar systems, Photochem. Photobiol. 28 (1978) 95–96.
[94] T. Miki, Y. Orii, The reaction of horseradish peroxidase with hydroperoxides derived from Triton X-100, Anal. Biochem. 146 (1984) 28–34.
[95] R.B. Woodward, V. Skaric, A new aspect of the chemistry of chlorins, J. Am. Chem. Soc. 83 (1961) 4676–4678.